

Hyperdynamics simulations with *ab initio* forces

Cite as: J. Chem. Phys. 154, 214112 (2021); doi: 10.1063/5.0047669

Submitted: 16 February 2021 • Accepted: 14 May 2021 •

Published Online: 4 June 2021



View Online



Export Citation



CrossMark

Hong-Yang Gu,^{1,2} Weiguo Gao,^{3,4} and Xin-Gao Gong^{1,2,a)}

AFFILIATIONS

¹ Key Laboratory for Computational Physical Sciences (MOE), State Key Laboratory of Surface Physics, Department of Physics, Fudan University, Shanghai 200433, China

² Shanghai Qizhi Institution, Shanghai 200232, People's Republic of China

³ School of Mathematical Sciences, Fudan University, Shanghai 200433, China

⁴ School of Data Science, Fudan University, Shanghai 200433, China

^{a)} Author to whom correspondence should be addressed: xggong@fudan.edu.cn

ABSTRACT

By applying the locally optimal rotation method to deal with the lowest eigenvalue of a Hessian matrix, we have efficiently incorporated the hyperdynamics method into the *ab initio* scheme. In the present method, we only need to calculate the first derivative of the potential and several more force calls in each molecular dynamics (MD) step, which makes hyperdynamics simulation applicable in *ab initio* MD simulations. With this implementation, we are able to simulate defect diffusion in silicon with boost factors up to 10^5 . We utilized both direct MD and the hyperdynamics method to investigate diffusion of lithium atoms and silicon vacancies in silicon. We identified the complex diffusion process. The obtained diffusion coefficients of Li atoms and Si vacancies are in good agreement with the direct MD results.

Published under an exclusive license by AIP Publishing. <https://doi.org/10.1063/5.0047669>

I. INTRODUCTION

Molecular dynamics (MD) simulation is a powerful tool to simulate dynamic processes and is widely used in systems with time scales of nanoseconds.^{1–5} However, for rare events, due to the long time scale, it is almost impossible to directly use a brute force method to calculate physical properties. In these systems, one does not care about realistic dynamical trajectories, rather we are only interested in some average dynamical probability, such as the rate constants.⁶ If the simulation time between the infrequent events can be sped up, it will be possible to use simulations to compute the probability of escape from the potential basin. Several solutions have been proposed to tackle this problem.^{6–9} Methods such as the bond-boost method¹⁰ and variable-driven hyperdynamics,¹¹ developed within the framework of hyperdynamics, have proved efficient for real systems. Most of these methods used an empirical potential to describe the many-body system and obtained relatively accurate results consistent with the direct MD results. They applied some approximations to the bias potential and simplified the estimation of the bias forces. However, these methods can hardly be applicable to real materials, where accurate force calculation is necessary.

The key for the success of hyperdynamics developed by Voter is to define a good bias potential,^{6,7,12} which ensures that the relative transition rates are unchanged.⁶ The bias potential can be defined as a function of the lowest eigenvalue of the Hessian matrix (ε_1)

and the projection of the first derivative of the potential along the eigenvector corresponding to ε_1 (g_{1p}). The eigenvalue ε_1 determines whether the system is near a saddle point, and a significant portion of the computational time is spent calculating this eigenvalue. For systems that are intrinsically local in their behavior, such as ion diffusion, one can define a proper environment and apply the local approximation to the system.^{13,14} The computational cost of dealing with the Hessian matrix is considerably reduced and is independent of the total number of the atoms in the simulation cell. In *ab initio* MD, it is difficult to calculate the Hessian matrix directly, and the finite difference method is too time-consuming to obtain meaningful results. The well-known dimer method constructs a dimer and delicately transforms the dilemma of solving for a matrix eigenvalue into a multivariate function optimization problem.^{15,16} However, in previous tests, the conjugate gradient (CG) used in the dimer method sometimes shows slow convergence or even diverges in restricted steps.^{17,18} This obstructs the accurate description of the potential energy surface and impairs computational efficiency.

In this paper, we develop a practical *ab initio* hyperdynamics method by implementing the Locally Optimal Rotation (LOR) method for finding a saddle point,¹⁸ and as applications, we simulate the diffusion of a Li atom and a vacancy in diamond Si. The resulting diffusion coefficients and the diffusion trajectories extracted from hyperdynamics simulations are in agreement with the direct MD

results. This indicates that our method is applicable to simulations of real materials and can notably reach low temperatures, which is forbidden for direct MD simulations.

II. HYPERDYNAMICS WITH A LOCAL BIAS POTENTIAL

In hyperdynamics as proposed by Voter,^{6,7} the simulation is performed on a modified potential $V_m(R)$, which equals the original potential $V(R)$ but adds a non-negative bias potential $V_b(R)$, i.e.,

$$V_m(R) = V(R) + V_b(R). \quad (1)$$

The bias potential needs to satisfy the requirement that $V_b(R) = 0$ in transition state regions,^{6,7} because it should not change the potential on the dividing surface and should preserve the relative transition escape rates. Applying transition state theory (TST), one can calculate the boost factor corresponding to the $V_b(R)$ and the accelerated time achieved by the hyperdynamics method,^{6,7}

$$t = \sum_{i=1}^n \Delta t_{MD} e^{\beta V_b(R_i)}, \quad (2)$$

where Δt_{MD} is the MD time step and n is the number of integration steps. Based on the local definition of TST boundaries,¹⁹ one can construct a bias potential $V_b(R)$ such as

$$V_b(R) = \frac{h}{2} \left[1 + \varepsilon_1 \left(\varepsilon_1^2 + \frac{|g_{1p}|^{1/n}}{d^2} \right)^{-\frac{1}{2}} \right]. \quad (3)$$

When the system reaches the dividing surface, $\varepsilon_1 < 0$, $g_{1p} = 0$, and $V_b(R) = 0$, and the potential in the transition states stays unchanged. The parameter h in the function denotes the bias potential height, and the parameter d is related to the width of the potential basin. The parameter n tunes the bias potential to avoid a sharp change in it. When the system is near some potential surface minimum, where $\varepsilon_1 > 0$, a comparatively large bias potential is added to the original potential and a relatively large boost factor is obtained. The non-negative bias enhances the escape rates and helps the system leave the current energy minimum. It should be noted that we employed the local approximation to construct the bias potential. This may cause discontinuities in potential energy surface (PES); however, such discontinuities will not harm the relative transition states in the hyperdynamics method¹² since the energy itself is not a conservation quantity in the simulation.

III. LOCALLY OPTIMAL ROTATION METHOD

Each integration step in hyperdynamics is quite heavy computationally compared to the direct MD simulation step. Most of the computational cost is spent dealing with the Hessian matrix to get ε_1 . In fact, it is very difficult to calculate the Hessian matrix directly. However, if the potential energy surface can be treated as a quadratic within a small region ΔR , one can construct a dimer of $R + \Delta R$ and $R - \Delta R$, about the midpoint, and the lowest eigenvalue can be numerically expressed as^{15,18}

$$\varepsilon_{1N} = \frac{V(R + \Delta R) + V(R - \Delta R) - 2V(R)}{(\Delta R)^2}. \quad (4)$$

According to the expression, minimizing ε_{1N} is equivalent to minimizing $V(R + \Delta R) + V(R - \Delta R)$, and this optimization can be solved without knowing the second derivatives of the potential. In order to solve this multivariate function optimization problem efficiently, we utilize the LOR method.¹⁸ Compared with the widely used modified CG method, in each rotation (except the initial one), the LOR method minimizes a 3×3 sub-eigenproblem instead of the 2×2 sub-eigenproblem,

$$\begin{aligned} (a^k b^k c^k) = \arg \min_{\|aN^{(k)} + b\Phi^{(k)} + cP^{(k)} = 1\|} (a b c) \begin{pmatrix} N^{(k)T} \\ \Phi^{(k)T} \\ P^{(k)T} \end{pmatrix} \\ \times H(N^{(k)} \Phi^{(k)} P^{(k)}) \begin{pmatrix} a \\ b \\ c \end{pmatrix}, \end{aligned} \quad (5)$$

where $N^{(k)} = \frac{\Delta R}{\|\Delta R\|}$ is the direction vector along the dimer, $\Phi^{(k)} = \frac{F(R+\Delta R) - F(R-\Delta R)}{\|F(R+\Delta R) - F(R-\Delta R)\|}$ is the unit vector parallel to the gradient, and $P^{(k)}$ is the imposed additional vector, which in each rotation is updated by

$$P^{(k+1)} = \frac{b\Phi^{(k)} + cP^{(k)}}{\|b\Phi^{(k)} + cP^{(k)}\|}. \quad (6)$$

For each rotation, the new dimer direction is determined by

$$N^{(k+1)} = a^k N^{(k)} + b^k \Phi^{(k)} + c^k P^{(k)}. \quad (7)$$

As a result, we do not need to apply the finite difference to calculate the $HN^{(k+1)}$. This matrix element can be obtained by the translation

$$HN^{(k+1)} = a^k HN^{(k)} + b^k H\Phi^{(k)} + c^k HP^{(k)}. \quad (8)$$

A similar translation also holds for $HP^{(k)}$. So, in each iteration, an extra force calculation is only required for $H\Phi^{(k)}$. Compared with the original dimer method, we only need half of the force calls in each iteration. This new strategy not only raises the convergence efficiency but also improves the numerical stability. The reason is that the translation will keep the direction when the sequence is close to convergence.

IV. DETAILS OF CALCULATIONS

We implemented the hyperdynamics scheme along with the LOR method in VASP code,²⁰ and thus, the *ab initio* molecular dynamics simulations with hyperdynamics can be performed. We used the projector-augmented wave (PAW)²¹ with the Perdew–Burke–Ernzerhof (PBE)²² exchange-correlation functional to perform the simulations. The cutoff energy for the plane-wave basis was 280 eV, and the energy convergence parameter was set to 10^{-8} eV due to the high precision requirement in bias force calculations. The silicon supercell contains 64 atoms, with one lithium atom added for lithium diffusion or one silicon atom removed for vacancy

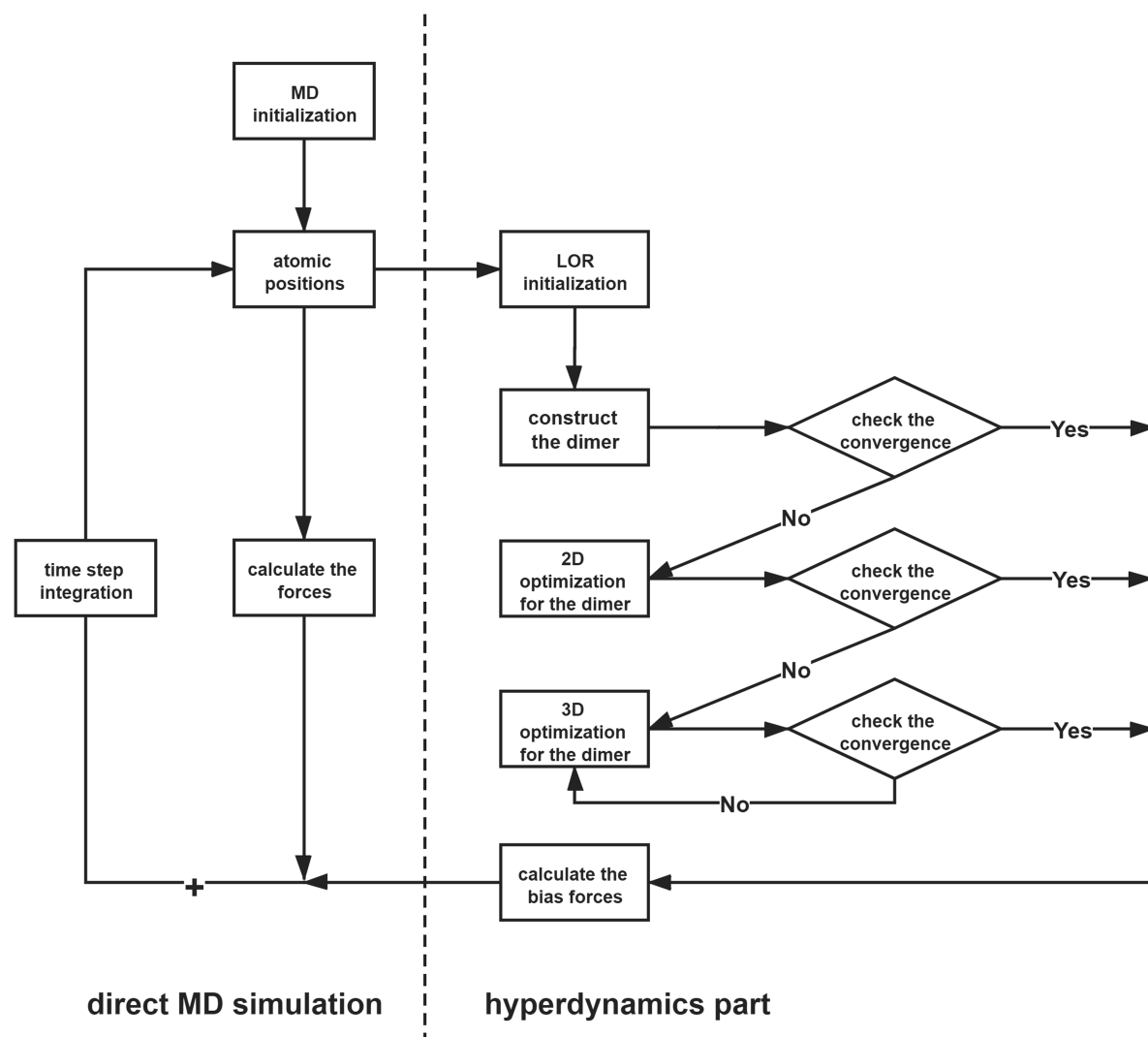


FIG. 1. The flow chart of the present hyperdynamics scheme. The left part is the direct MD simulation, and the right part belongs to the bias force calculation in hyperdynamics. The most computationally heavy part is determining the softest mode in the Hessian matrix.

diffusion. We chose the Li_sv pseudo-potential to treat the semi-core 1s states as valence states and used a k-point mesh of $1 \times 1 \times 1$ for all simulations.

For the direct MD simulations, the time step was 1 fs, and each simulation lasted for 40 ps, where the first 5 ps were used for the systems to reach the equilibrium state. As for hyperdynamics, the systems were allowed to achieve equilibrium for 1000 hyperdynamics steps with a time step of 1.5 fs, and further 6 ps were subsequently utilized to form averages in the simulations. The Nose–Hoover thermostat²³ was employed in order to control the system at different finite temperatures.

When the LOR optimization was executed, the rotations were stopped if the residual corresponding to the dimer direction vector was less than 0.1 eV/Å. The initial mode for the dimer was set randomly in the first MD step. For the later MD steps, the initial mode

was constructed according to the optimized mode of the last MD step. The calculation flow of our hyperdynamics scheme is shown in Fig. 1.

V. RESULTS

A. Lithium atom diffusion in bulk silicon

Si is a common negative electrode material in commercial Li-ion batteries.^{24–26} Due to having the highest theoretical capacity, lithium metal is the ultimate choice for the anode in the Li battery.²⁷ Therefore, it is crucial to determine the dynamical properties of Li diffusion in Si. Experimental and theoretical work focused on this topic since the 1960s.^{28–31} In the density functional theory (DFT) calculations, the NEB method³² was used to determine the diffusion path and the energy barrier. It is a common belief that the tetrahedral

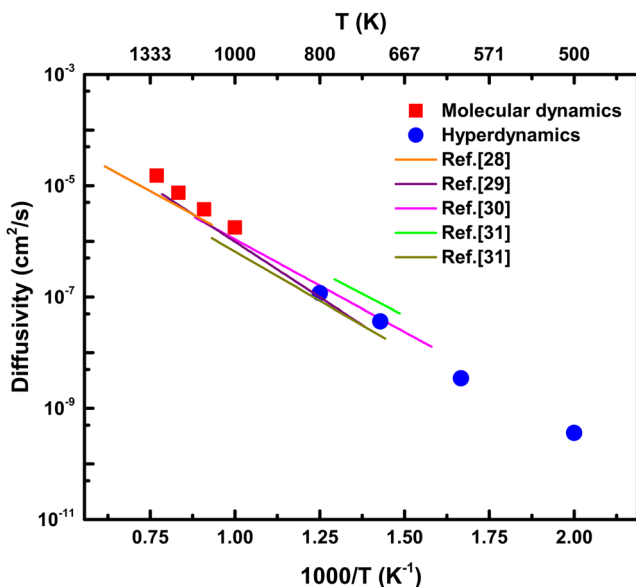


FIG. 2. The temperature-dependent diffusion coefficient for lithium in silicon. The red square dots are the diffusion results from the direct MD, and the blue round dots are from hyperdynamics simulations. The colored straight lines are experimental results in 1950s or 1960s.^{28–31} The hyperdynamics simulation results at low temperature is in good agreement with both the direct MD at high temperature and experiments.

(T_d) site is the most stable site for a lithium atom in bulk silicon.³³ The NEB method yielded the result that the lithium diffused from one T_d site to the nearest T_d site along the T_d-Hex-T_d pathway.³³ The reported NEB energy barrier for this diffusion pathway is about 0.55–0.60 eV,^{33–35} which is generally lower than the experiment barrier height (0.57–0.79 eV).^{28–31,36} This indicates that the diffusion properties of lithium atoms at finite temperature may not be well described by the static calculations. In order to understand the diffusion behavior of Li in silicon, we performed *ab initio* hyperdynamics to demonstrate our scheme and did a detailed analysis of the MD and hyperdynamics diffusion trajectories.

In our hyperdynamics simulations, we set the Li atom and the nearest 30 atoms as the local environment. We performed direct

MD simulations at a high temperature from 1000 to 1300 K and the hyperdynamics from 500 to 800 K. The mean square displacements (MSDs) of the Li atoms were calculated to obtain the diffusion coefficient at different temperatures,

$$D = \frac{1}{6t} \langle (r(t + t_0) - r(t))^2 \rangle, \quad (9)$$

where D is the diffusion coefficient. In direct MD, t is the corresponding MD simulation time ($t = \sum \Delta t_{MD}$). While in hyperdynamics, t denotes the accelerated time, which equals the MD simulation time scaled by the average boost factor [$t = (\sum \Delta t_{MD})BF$]. The diffusion constants shown in Fig. 2 are the average results of the bias potential with a different set of parameters ($h = 0.575, 0.55$ eV, $d = 1.75, 2$). Our NEB calculation result showed that the energy barrier is 0.61 eV of the T_d-Hex-T_d diffusion path. The chosen parameters will not change the diffusion properties of the Li atom.

As can be seen in Fig. 2, our conventional MD results at high temperature (1000–1300 K) are close to experimental data, which indicates that the present simulation method is able to describe this system. The diffusion coefficients from hyperdynamics and direct MD simulations are closely consistent and aggregated yield the activation energy, $E = (0.76 \pm 0.02)$ eV, which is larger than that of the NEB calculation. The difference between the NEB barrier and the MD calculated barrier mainly could come from the fact that the physical properties associated with the finite temperature effect are ignored in the static NEB calculation.³⁷

Based on the relative position of the initial T_d site and the final T_d site of the real diffusion trajectories, we found that the majority of diffusion trajectories are similar to the path predicted by the NEB calculation [Fig. 3(a)], although the visible difference can be observed. In addition to the usual diffusion pathway, we also observed two other unusual pathways. In the second pathway, the Li atom can reach the next nearest T_d site without passing by the nearest T_d site [Fig. 3(b)]. Moreover, in the third path [Fig. 3(c)], the Li atom can even pass through the bond center to another T_d site. We also did the NEB calculations for those paths identified in MD simulation. The result of the first diffusion path is identical to the NEB result with the lowest barrier [Fig. 4(a)], where the calculated barrier is 0.61 eV and similar to previous calculations.^{33–35} The second path yields a high barrier (1.40 eV) in the NEB calculation,

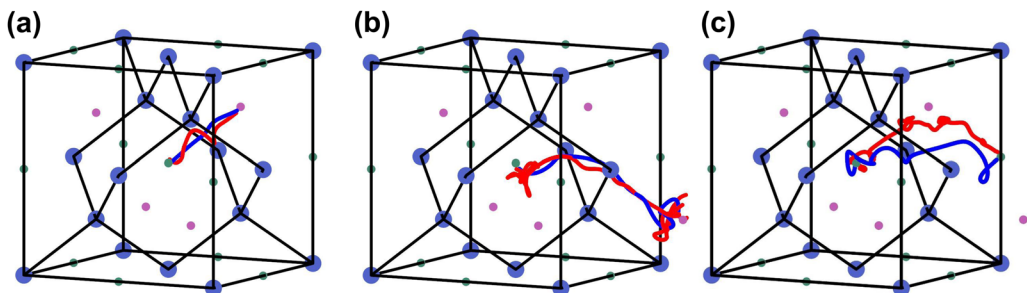


FIG. 3. Diffusion trajectories of the lithium atom in silicon. The red lines are trajectories extracted from MD simulations, and the blue lines are from hyperdynamics simulations. (a) is similar to the pathway yielded by the NEB method, where the atom diffuses from a T_d site to the nearest T_d site. Besides, the atom moves directly to the second nearest T_d site in (b) and passes through the bond center in (c). The real trajectories are not identical to the static diffusion pathway.

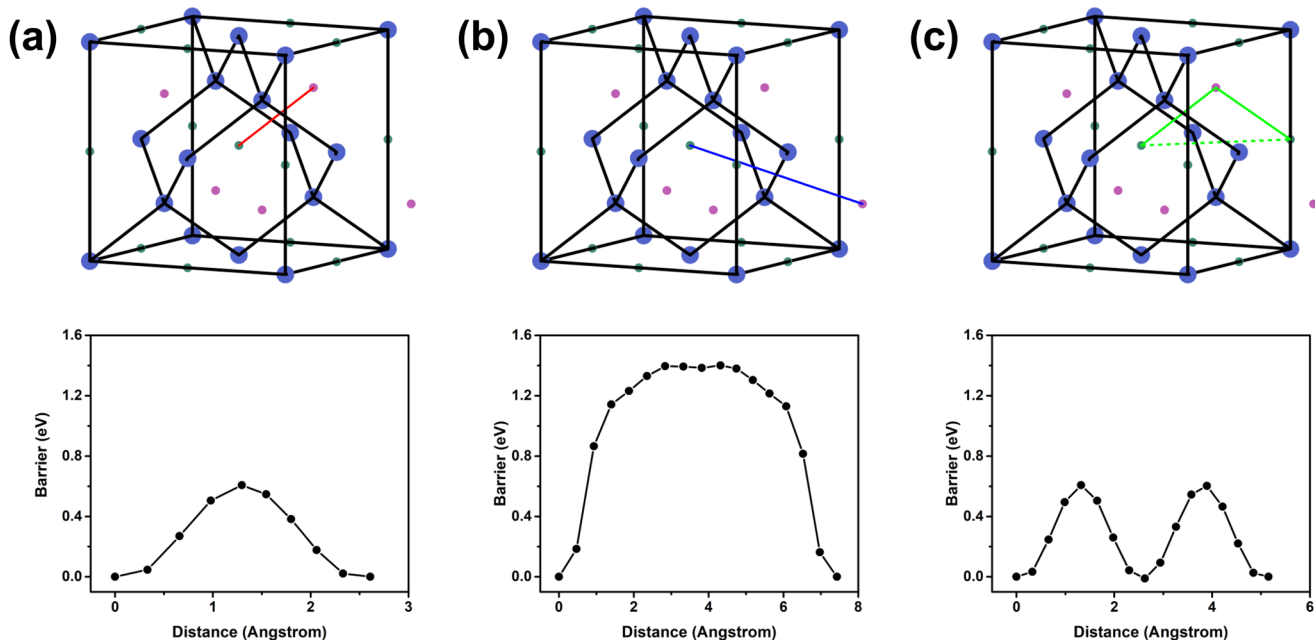


FIG. 4. NEB calculations of the diffusion pathways of the lithium atom. The figures below are the corresponding NEB calculated barrier results of the pathway illustrated above. The first diffusion path showed in (a) is identical to the NEB result. The second one showed in (b) has a relatively high energy barrier, which can only be observed in the dynamics simulations. In the third pathway (c), the lithium atom moves directly along the $\langle 110 \rangle$ direction, which is equivalent to the successive translations of path 1. The diffusion process with the higher barrier is irrelevant in TST.

which is significantly larger than the lowest NEB barrier. According to classical transition state theory, at 500 K, the diffusion constant associated with this path is estimated as eight orders of magnitude lower than that of the first pathway. At a high temperature of 1300 K, it is still lower by about three orders. The diffusion along this path would be extremely rare, actually no contribution to the diffusion constant. For the third pathway, the unstable intermediate configuration makes the NEB trajectory regress to the combination of the two first paths.

It is worth noting that the hyperdynamics method focuses on the transition rates and is not able to give the detailed description of the trajectories, due to the effect from the bias potential. It was known that the DFT can give the inaccurate estimation of the barrier heights associated with the transition states,³⁸ and the finite-size effect in MD simulations also affects the accuracy of the diffusion coefficient.³⁹ The very accurate migration barrier cannot be expected from the *ab initio* dynamics simulations.

In the hyperdynamics simulations for Li adatom diffusion, the average rotations needed in each optimization of the lowest eigenvalue of the Hessian matrix are 5.5, so the average force calls required in each MD step are 9.5, while the boost factor we obtained is from 10^2 to 10^5 in the simulation temperature range, and the boost factor increases with the reduction in temperature. This indicates that we can get a 10^2 – 10^5 fold speedup at the expense of less than one-tenth times the computation effort in each integration step. It is almost impossible to get reasonable results in the low temperature region without the bias potential due to the diffusion coefficient being orders of magnitude lower.

B. Vacancy diffusion in bulk silicon

Self-diffusion in bulk silicon is contributed to both vacancy and self-interstitial diffusion.⁴⁰ Although the diffusion barrier was determined decades ago⁴¹ and the precision has been improved by recent experimental results,^{40,42,43} the detailed activation mechanisms associated with vacancies and self-interstitials are still in controversial discussion.⁴⁴ *Ab initio* MD results for vacancy diffusion are still lacking due to the long simulation time to establish equilibrium.

We simulated silicon vacancies using the hyperdynamics method. Unlike the situation in adatom diffusion, the local environment is not easily identified for vacancy diffusion. In order to obtain the appropriate Hessian matrix information of the local environment, we define the coordinate of the vacancy according to the four nearest silicon atoms as follows (Fig. 5):

$$\vec{R} = \vec{R}_0 + \frac{\sum \lambda_i |\vec{R}_i|}{\sum \lambda_i}, \quad \lambda_i = \frac{1}{|\vec{R}_i|^2}, \quad (10)$$

where \vec{R}_i is the coordinate of the four nearest silicon atoms and \vec{R}_0 is the origin lattice point of the vacancy. If we detect that $|\vec{R}_i|_{min} < \frac{r_{bond}}{2}$, we deem that vacancy migration has happened and another four nearest atoms will be newly labeled to determine the current vacancy coordinate. The detailed description of the algorithm to determine the four nearest silicon atoms is given in the [supplementary material](#). The diffusion barrier for the vacancy is the sum of the formation energy and the migration barrier. In our dynamic simulations, we only focused on the migration barrier.

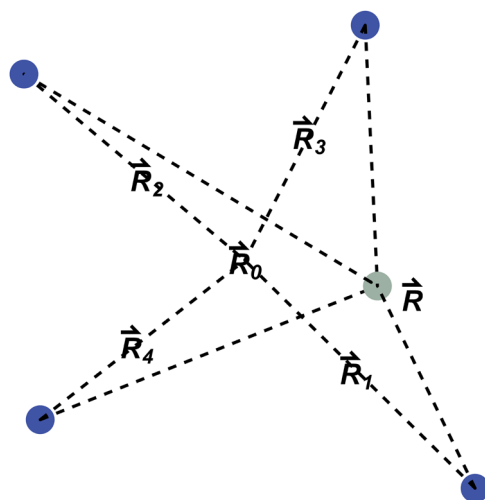


FIG. 5. The method to define the coordinate of the vacancy according to the four nearest silicon atoms. Blue points denote the four nearest silicon atoms, and \vec{R}_0 is the origin lattice point of the vacancy. We can calculate the vacancy coordinate based on the weighted average of each bond.

As in the lithium diffusion test, we chose another set of parameters ($h = 0.3, 0.275$ eV, $d = 1.25, 1$) in the bias potential and calculated the average results for these parameters. The strength of the bias potential was also guaranteed to be less than the NEB calculated barrier.⁴⁵ We performed the direct MD simulation from 700 to 1000 K and the hyperdynamics simulation from 500 to 650 K (Fig. 6). The maximum boost factor obtained through the

simulation is around 35, and the average force calls needed in each integration step are 7.2. Although the acceleration effect is not as obvious as that in the case of adatom diffusion, hyperdynamics is still necessary in the low temperature region.

The diffusion pathway observed by the dynamics simulation is identical to the pathway determined by the NEB calculation. In the dynamics simulations, this is the only diffusion mechanism we obtained. The vacancy hopped to a nearest neighbor site. One of the nearest silicon atoms moves along the $\langle 111 \rangle$ direction toward the vacancy site and fails into the original site occupied by the vacancy. The activation energy fitted by the diffusion coefficient is (0.35 ± 0.03) eV. The result is similar to the previously reported theoretical predictions (0.33–0.40 eV),^{45–47} according to empirical MD simulations or NEB calculations. This demonstrates the flexibility of our hyperdynamics scheme, which can be applied to vacancy systems.

VI. SUMMARY

We have developed the hyperdynamics method within the *ab initio* scheme with the implementation of the LOR method. We demonstrated that such *ab initio* hyperdynamics are applicable to real systems in the low temperature region, such as interstitials or vacancy diffusion, which was not reachable in the conventional *ab initio* MD. The obtained hyperdynamics results are in good agreement with the conventional MD simulations, which demonstrates the effectiveness of our simulations. Hyperdynamics can accelerate the simulation and enhance the escape rates from the potential basin by a factor of up to 10^5 . We believe that the algorithm will provide a route for the study of rare events and guide the development of defect dynamic simulations.

SUPPLEMENTARY MATERIAL

See the [supplementary material](#) for graphical representations of the bias potential and more calculation details of MD/hyperdynamics simulations.

ACKNOWLEDGMENTS

H.-Y. Gu would like to thank Dr. J. Wragg for polishing the manuscript. We acknowledge the stimulating discussion with Dr. Min Ji. X.-G.G. acknowledges funding support from the National Natural Science Foundation of China and the Science Challenge Project (Grant No. TZ2018004). W.G. acknowledges funding support from the National Natural Science Foundation of China (Grant Nos. 11690013 and U1811461) and the National Key R & D Program of China (Grant No. 2020YFA0711902). Calculations are performed at the Supercomputer Center of Fudan University.

DATA AVAILABILITY

The data that support the findings of this study are available from the corresponding author upon reasonable request.

REFERENCES

- ¹R. Car and M. Parrinello, *Phys. Rev. Lett.* **55**, 2471 (1985).
- ²M. Karplus and G. A. Petsko, *Nature* **347**, 631 (1990).

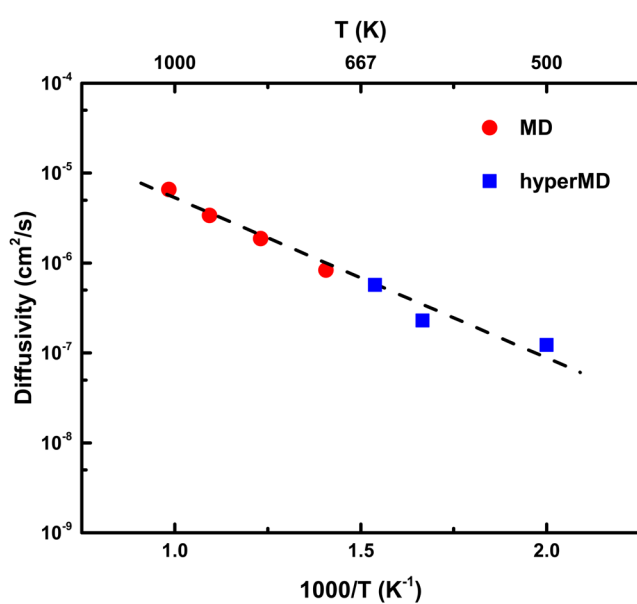


FIG. 6. The temperature-dependent diffusion coefficient for silicon vacancy. The dashed line is the fitting result combined with the direct MD at high temperature and hyperdynamics in the low temperature region. The present hyperdynamics scheme can be applicable to vacancy systems.

- ³G. Kresse and J. Hafner, *Phys. Rev. B* **47**, 558 (1993).
- ⁴J. C. Phillips *et al.*, *J. Comput. Chem.* **26**, 1781 (2005).
- ⁵S. Nosé and M. L. Klein, *Mol. Phys.* **50**, 1055 (2006).
- ⁶A. F. Voter, *Phys. Rev. Lett.* **78**, 3908 (1997).
- ⁷A. F. Voter, *J. Chem. Phys.* **106**, 4665 (1997).
- ⁸M. R. Sørensen and A. F. Voter, *J. Chem. Phys.* **112**, 9599 (2000).
- ⁹G. Henkelman and H. Jónsson, *J. Chem. Phys.* **115**, 9657 (2001).
- ¹⁰R. A. Miron and K. A. Fichthorn, *J. Chem. Phys.* **119**, 6210 (2003).
- ¹¹K. M. Bal and E. C. Neyts, *J. Chem. Theory Comput.* **11**, 4545 (2015).
- ¹²S. Y. Kim, D. Perez, and A. F. Voter, *J. Chem. Phys.* **139**, 144110 (2013).
- ¹³X. G. Gong and J. W. Wilkins, *Phys. Rev. B* **59**, 54 (1999).
- ¹⁴X. M. Duan and X. G. Gong, *Comput. Mater. Sci.* **27**, 375 (2003).
- ¹⁵G. Henkelman and H. Jónsson, *J. Chem. Phys.* **111**, 7010 (1999).
- ¹⁶A. Heyden, A. T. Bell, and F. J. Keil, *J. Chem. Phys.* **123**, 224101 (2005).
- ¹⁷R. A. Olsen *et al.*, *J. Chem. Phys.* **121**, 9776 (2004).
- ¹⁸J. Leng *et al.*, *J. Chem. Phys.* **138**, 094110 (2013).
- ¹⁹E. M. Sevick, A. T. Bell, and D. N. Theodorou, *J. Chem. Phys.* **98**, 3196 (1993).
- ²⁰G. Kresse and J. Furthmüller, *Phys. Rev. B* **54**, 11169 (1996).
- ²¹P. E. Blöchl, *Phys. Rev. B* **50**, 17953 (1994).
- ²²J. P. Perdew, K. Burke, and M. Ernzerhof, *Phys. Rev. Lett.* **77**, 3865 (1996).
- ²³D. J. Evans and B. L. Holian, *J. Chem. Phys.* **83**, 4069 (1985).
- ²⁴M. Gauthier *et al.*, *Energy Environ. Sci.* **6**, 2145 (2013).
- ²⁵L. Lang *et al.*, *Nanoscale* **5**, 12394 (2013).
- ²⁶C. K. Chan *et al.*, *Nat. Nanotechnol.* **3**, 31 (2008).
- ²⁷D. Lin, Y. Liu, and Y. Cui, *Nat. Nanotechnol.* **12**, 194 (2017).
- ²⁸E. M. Pell, *J. Phys. Chem. Solids* **3**, 77 (1957).
- ²⁹C. S. Fuller and J. A. Ditzenberger, *Phys. Rev.* **91**, 193 (1953).
- ³⁰C. S. Fuller and J. C. Severiens, *Phys. Rev.* **96**, 21 (1954).
- ³¹A. Seeger and K. P. Chik, *Phys. Status Solidi B* **29**, 455 (1968).
- ³²G. Mills and H. Jónsson, *Phys. Rev. Lett.* **72**, 1124 (1994).
- ³³W. Wan *et al.*, *J. Phys.: Condens. Matter* **22**, 415501 (2010).
- ³⁴K. Zhao *et al.*, *Nano Lett.* **11**, 2962 (2011).
- ³⁵C.-Y. Chou, H. Kim, and G. S. Hwang, *J. Phys. Chem. C* **115**, 20018 (2011).
- ³⁶S. W. Jones, *Diffusion in Silicon* (IC Knowledge LLC, 2008).
- ³⁷R. Crehuet and M. J. Field, *J. Chem. Phys.* **118**, 9563 (2003).
- ³⁸S. A. Ghasemi *et al.*, *Phys. Rev. B* **81**, 214107 (2010).
- ³⁹S. H. Jamali *et al.*, *J. Chem. Theory Comput.* **14**, 2667 (2018).
- ⁴⁰T. Südkamp and H. Bracht, *Phys. Rev. B* **94**, 125208 (2016).
- ⁴¹P. M. Fahey, P. B. Griffin, and J. D. Plummer, *Rev. Mod. Phys.* **61**, 289 (1989).
- ⁴²E. Hüger *et al.*, *Phys. Status Solidi B* **249**, 2108 (2012).
- ⁴³R. Kube *et al.*, *Phys. Rev. B* **88**, 085206 (2013).
- ⁴⁴M. Suezawa, Y. Iijima, and I. Yonenaga, *Jpn. J. Appl. Phys., Part 1* **59**, 045505 (2020).
- ⁴⁵F. El-Mellouhi, N. Mousseau, and P. Ordejón, *Phys. Rev. B* **70**, 205202 (2004).
- ⁴⁶L. J. Munro and D. J. Wales, *Phys. Rev. B* **59**, 3969 (1999).
- ⁴⁷N. Bernstein and E. Kaxiras, *Phys. Rev. B* **56**, 10488 (1997).